Mesogenic lattice models with partly antinematic interactions producing uniaxial nematic phases

Giovanni De Matteis*
Centro di Ricerca Matematica "Ennio De Giorgi," Collegio Puteano, Scuola Normale Superiore di Pisa, Piazza dei Cavalieri 3, I-56100 Pisa, Italy

Silvano Romano†
Unità di Ricerca CNISM e Dipartimento di Fisica "A. Volta," Universitá di Pavia, Via A. Bassi 6, I-27100 Pavia, Italy
(Received 18 March 2009; published 8 September 2009)

The present paper considers nematogenic lattice models, involving particles of D_{2h} symmetry, whose centers of mass are associated with a three-dimensional simple cubic lattice; the pair potential is isotropic in orientation space and restricted to nearest neighbors. Let two orthonormal triads define orientations of a pair of interacting particles; the simplest potential models proposed in the literature can be reduced to a linear combination involving the squares of the scalar products between corresponding unit vectors only and depending on three parameters. By now, various sets of potential parameters have been proposed and studied in the literature, some of which capable of producing biaxial orientational order at sufficiently low temperature. On the other hand, in experimental terms, mesogenic biaxial molecules mostly produce uniaxial mesophases; thus we address here two very simple cases, involving a nematic (calamitic) term as well as one (model P0M) or two (model PPM) antinematic ones, whose coefficients are set equal in magnitude; when only one antinematic coefficient is used, the third one is set to zero. The calamitic term favors the alignment of two corresponding molecular axes, whereas antinematic terms or geometric constraints tend to keep two other pairs of axes mutually orthogonal. The models were investigated by molecular-field treatments and Monte Carlo simulation and found to predict a first- or second-order transitions between uniaxial nematic and isotropic phases; the molecular-field treatments yielded results in reasonable agreement with simulation.

DOI: 10.1103/PhysRevE.80.031702 PACS number(s): 61.30.Cz

I. INTRODUCTION

Although nematogenic molecules do not possess cylindrical symmetry and often have appreciable dipole moments, mesophases produced by low-molecular weight compounds are usually uniaxial and apolar; on this ground, in a number of cases, both theoretical treatments and interpretations of experimental results have been simplified by assuming from the start that nematogenic molecules possess uniaxial ($D_{\infty h}$) symmetry. On the other hand, the possible effects of molecular deviations from cylindrical symmetry (molecular biaxiality) on nematic order have been studied theoretically as well. Starting in 1970 [1] and by the end of the past century, approximate analytical theories such as molecular-field (MF) or Landau treatments, and later simulation studies had shown that single-component models consisting of molecules possessing D_{2h} symmetry, and interacting by various appropriate continuous or hard-core potentials can produce a biaxial phase; a more extensive treatment and a more detailed bibliography can be found, for example, in Refs. [2,3]; a review on computer simulation studies of (thermotropic) biaxial nematics has recently been published [4]. Here we just point out a few aspects of the research carried out so far: on the one hand, much theoretical or simulation work has addressed simple rigid-body models, but molecular flexibility has been allowed for in some cases, e.g., Ref. [5]; on the other hand, models based on continuous second-rank interactions only have often been studied, but in some very recent case [6], third-rank interactions have also been allowed for in bent-core models, producing tetrahedratic order. Moreover, rather simplified models have been used in most cases but an atomistic simulation of a mesogen showing evidence of biaxial behavior has been reported as well [7]. Let us finally recall that other theoretically predicted thermotropic mesophases (polar or other unconventional nematics, see below) seem to be still missing and are being sought for [4].

As for experimental realizations, a biaxial phase had been discovered in a lyotropic system in 1980 [8]; since 1986 and until approximately 2003, there had been numerous reports of thermotropic biaxiality in low-molecular weight compounds, many of which were later called into question [9–11]: this situation of claims and counterclaims is aptly summarized by the very titles of Refs. [9–11].

Better experimental evidence was produced since 2004 and by now for a few classes of compounds; see also Refs. [4,12] for a thorough discussion and a more detailed bibliography. In particular, there have been claims to have discovered a biaxial nematic phase in polar bent-core (banana-shaped) molecules [13–16] (but see also Refs. [17,18]) and for organosiloxane tetrapode molecules; the latter contain four identical mesogenic groups, tethered laterally via siloxane chains to a single silicon (Refs. [19–22]) or germanium core [23]. Hindrance of molecular rotation due to mesogen-core linkages or to interdigitation among mesogens connected to different cores is expected to favor biaxial order [23]. Evidence of thermotropic biaxial behavior has been found in polymeric systems [24–26] as well, and evidence of a direct first-order isotropic-to-biaxial transition in orthometallated (platinum) imine complexes has been reported in Ref.

*giovanni.dematteis@sns.it
†silvano.romano@pv.infn.it

[27]. Let us also mention that a possible alternative picture of biaxial nematic order [4,28] has been proposed based on the idea of biaxial domains reoriented by surface anchoring or external fields.

The experimental search for better evidence and for more realizations of the (thermotropic) biaxial nematic phase [29] continues to arise both excitement and interest and still an active scientific debate [4]; interest is also connected with its possible applications, for example in displays [4,30–32]: orientation of the secondary director in response to external perturbations is expected to be significantly faster than for the primary one.

Also starting a few years ago, i.e., simultaneously with and independently of the named experimental work, a renewed theoretical study of simple continuous biaxial mesogenic models was undertaken in Refs. [33–37]; the proposed models were studied by MF, Monte Carlo simulation (MC) [3,38,39], and, in some cases, by two-site cluster theory [40]. Moreover, very recently and motivated by the above experimental facts, the single-tensor Landau–de Gennes theory of biaxial nematics has been carefully reexamined in Ref. [41] and a double-tensor Landau theory has been put forward and studied in Refs. [42,43]; an extensive symmetry analysis of unconventional nematic phases, i.e., associated with the onset of either one tensor of rank different from 2 or of several combined tensors, was recently developed in Refs. [43–45].

Partly continuing along this line, we consider here a nematogenic lattice model, where the pair potential is restricted to nearest neighbors, and has the simplified functional form recently proposed by Durand, De Matteis, Sonnet, and Virga (DDSV) [33,34] or rather an extreme case thereof. The resulting behavior is investigated by MF, and comparisons are made with MC simulations. More precisely, since thermotropic biaxial nematic behavior is the exception rather than the rule, and on the other hand, the pair potential model to be used is rather versatile (see below), our main purpose is to single out specific cases of the general pair potential, expected to produce a uniaxial and not biaxial ground state.

Over the decades, mesophases possessing no positional order, such as the nematic one, have often and quite fruitfully been studied by means of lattice models involving continuous interaction potentials (see Refs. [46,47]), starting with the seminal Lebwohl-Lasher simulation paper in the early 1970s (see Ref. [48]). As noted, for example, in Ref. [47], usage of a lattice model produces significant savings in computational terms; moreover, it entails that a number of competing phases (e.g., smectic ones), possibly pre-empting the nematic one, are excluded from the start; notice that similar simplifications as for the possible phases are used in other named theoretical treatments as well. Let us also mention in passing that, in some other cases, where the possibility of smectic order is allowed for, the treatment has been simplified by taking the long molecular axes to be taken to be fully aligned so that the isotropic liquid is eliminated [49,50].

II. PAIR POTENTIAL AND GROUND STATE

We are considering here classical identical particles, possessing D_{2h} symmetry, whose centers of mass are associated with a three-dimensional simple cubic lattice $\mathbb{Z}^3$; let $\mathbf{x}_\chi \in \mathbb{Z}^3$ denote the coordinate vectors of their centers of mass. Notice that the lattice is bipartite: one can define the parity of each site via the sum of its three coordinates so that, for each lattice site, all its nearest neighbors have opposite parity, all next-nearest neighbors have the same parity and so on.

The interaction potential is isotropic in orientation space and restricted to nearest neighbors, involving particles or sites labeled by χ and ρ, respectively; the orientation of each particle can be specified via an orthonormal triplet of three-component vectors (e.g., eigenvectors of its inertia tensor), say $\{\mathbf{n}_{\chi,j}, j=1,2,3\}$; in turn these are defined by an ordered triplet of Euler angles $\omega_\chi=\{\phi_\chi, \theta_\chi, \psi_\chi\}$; orientations are defined with respect to a common, but otherwise arbitrary, Cartesian frame. It also proves convenient to use a simpler notation for the unit vectors defining orientations of two interacting molecules [51], i.e., $\mathbf{u}_j$ for $\mathbf{n}_{\chi,j}$ and $\mathbf{v}_k$ for $\mathbf{n}_{\rho,k}$, respectively; here, for each j, $\mathbf{u}_j$ and $\mathbf{v}_j$ have the same functional dependences on ω_χ and ω_ρ, respectively (pairs of corresponding unit vectors in the two interacting molecules); let $\tilde{\Omega}=\Omega_{\chi\rho}$ denote the set of Euler angles defining the rotation transforming $\mathbf{u}_j$ into $\mathbf{v}_j$; Euler angles will be defined here according to the convention used by Brink and Satchler [52–54]. We also define

$$f_{jk} = (\mathbf{v}_j \cdot \mathbf{u}_k), \quad G_{jk} = P_2(f_{jk}), \tag{1}$$

where $P_2(\ldots)$ denotes the second Legendre polynomial.

The simplest continuous interaction potentials proposed and studied in this context (see, e.g., Refs. [33,34,55,56]) are quadratic with respect to the scalar products f_{jk}; owing to available geometric identities and without any loss of generality (see, e.g., the discussion in Ref. [3]), they can be reduced to a linear combination involving the three terms G_{kk} only, i.e.,

$$\Phi = \epsilon \sum_{k=1}^{3} r_k G_{kk} \tag{2a}$$

or

$$\Phi = \epsilon\{\xi G_{33} + \eta(G_{11} - G_{22}) + \zeta[2(G_{11} + G_{22}) - G_{33}]\}. \tag{2b}$$

Here ϵ is a positive quantity, setting energy and temperature scales (i.e., $T^*=k_BT/\epsilon$); linear transformations between the two sets of coupling constants can be found in Ref. [3]; notice also that the parameter space can be significantly reduced, allowing for duality, i.e., invariance of the pair potential upon applying the same permutation to both sets of interacting axes (see Refs. [3,33,34]); moreover, the three coefficients in each set can be taken to be smaller than 1 in magnitude, possibly at the cost of rescaling ϵ, and hence the temperature.

Particle interactions, correlations, and orientational order are usually expressed in terms of symmetry-adapted combinations of Wigner rotation functions $\mathcal{D}^J_{m,n}(\omega)$, i.e., for D_{2h} symmetry (see, e.g., Refs. [51,57,58], as well as detailed comparisons and discussion of notational issues in Ref. [59])

$$R^J_{pq}(\omega) = (1/4) \sum_{s=\pm 1} \sum_{t=\pm 1} \mathcal{D}^J_{sp,tq}(\omega). \tag{3}$$

Here J, p, and q denote even and non-negative integers, $0 \le p \le J$, $0 \le q \le J$, and $\omega = \{\phi, \theta, \psi\}$ denote the ordered triplet of Euler angles; thus

$$R^2_{00}(\omega) = P_2(\cos\ \theta),$$

$$R^2_{02}(\omega) = (1/4)\sqrt{6}\ \sin^2\ \theta \cos(2\psi),$$

$$R^2_{20}(\omega) = (1/4)\sqrt{6}\ \sin^2\theta \cos(2\phi),$$

$$R^2_{22}(\omega) = (1/4)(1 + \cos^2\ \theta)[\cos(2\phi)\cos(2\psi)] - (1/2)\cos\ \theta[\sin(2\phi)\sin(2\psi)]. \tag{4}$$

Each term G_{jk} can be expressed as a linear combination of the four above functions $R^2_{pq}(\tilde{\Omega})$ (see, e.g., Refs. [3,58]). Moreover, it proves notationally convenient, especially in view of a MF treatment, to define the simpler symbols $s_k(\omega)$ as well, involving just one subscript, thus

$$s_1(\omega) = R^2_{00}(\omega), \quad s_2(\omega) = R^2_{20}(\omega),$$

$$s_3(\omega) = R^2_{02}(\omega), \quad s_4(\omega) = R^2_{22}(\omega). \tag{5}$$

The rather general potential model to be considered [Eqs. (1)] can also be written in terms of the above symmetry-adapted basis functions [Eqs. (4) and (5); see also remarks on notation in Ref. [2]], i.e.,

$$\Phi = \epsilon \left\{ \xi s_1(\tilde{\Omega}) - \frac{\sqrt{6}}{2}\eta[s_2(\tilde{\Omega}) + s_3(\tilde{\Omega})] + 6\zeta s_4(\tilde{\Omega}) \right\}. \tag{6}$$

Over the years, various specific parameterizations had been proposed and studied for Eqs. (1); one of them, due to Straley [55] is based on an approximate mapping from a hard-parallelepiped model; another, more often studied one, is $\xi = -1$, $4\zeta = -\eta^2$; this can also be obtained by starting from a dispersion model at the London-de Boer-Heller approximation [60,61] and isotropically averaging over the orientation of the intermolecular vector (see, e.g., Refs. [56,62]); models with fully anisotropic dispersion interactions restricted to nearest neighbors and associated with both two- and three-dimensional lattices have been studied as well [63,64].

Both the Straley model [55] and the "dispersive" one mostly predict a biaxial-to-uniaxial transition of second order, followed by a uniaxial-to-isotropic transition of first order; a direct biaxial-to-isotropic transition of second order only exists for special values of the potential parameters (isolated Landau points). A new approach was proposed over the last few years by DDSV; in their study, the named authors [33,34] had examined, for general values of the parameters, the mathematical conditions under which the pair potential [Eqs. (1)] produces a fully aligned biaxial pair ground state, as well as its mechanical stability; the named stability condition [33,34] reads as

$$\zeta < 0, \quad \text{and} \quad |\eta| < -(\xi + \zeta). \tag{7}$$

Moreover, the named authors had proposed the simplified model defined by $\xi = -1$, $\eta = 0$, $\zeta < 0$, i.e., $r_1 = r_2$ (entailing an additional D_{4h} symmetry of the interaction [2]), and studied it by MF, carrying out a bifurcation analysis of the resulting consistency equations; the existence of direct transitions between biaxial and isotropic phases was proven, together with criteria for the existence of tricritical points.

An extensive study of the more general potential model [i.e., $\eta \neq 0$ in Eq. (2b)] by bifurcation theory (as proposed in Ref. [65] and then in Ref. [58]) can be found in Refs. [66,67]. MF and simulation studies of the general model, with parameters in the above biaxial stability region [Eq. (7)], can be found in Ref. [68]. A later MF treatment [69] carried out comparison between the complete potential model and its simplified version ($\eta = 0$) over appropriate parameter ranges where they both support a uniaxial as well as biaxial phase; it was found that the ratio between the two transition temperatures is weakly dependent on η; in this sense, the simplified potential model yields the dominant biaxial quadrupolar contribution to the nematic potential of mean torque [69].

Yet, in experimental terms, the thermotropic biaxial phase is an exception rather than the rule, and on the other hand, the presence of three coupling constants in Eqs. (1) makes the pair potential model under consideration capable of producing different types of orientational order in the pair ground state and hence in low-temperature phases; thus, there is some interest in addressing regions of the parameter space where sizable antinematic terms prevent the existence of a biaxially ordered pair ground state; this range is defined in general by [2,33–36]:

$$\zeta \ge 0, \quad \text{and} \quad |\eta| \ge -(\xi + \zeta). \tag{8}$$

We address here a family of potential models defined in general by

$$r_1 \ge 0, \quad r_2 \ge 0, \quad r_1 + r_2 > 0, \quad r_3 < 0 \tag{9}$$

in Eq. (2a) and, more explicitly, two very simple examples of it. One of them (P0M) is defined by $r_1 = +1$, $r_2 = 0$, and $r_3 = -1$ in Eq. (2a), i.e., $\xi = -\frac{3}{4}$, , $\eta = +\frac{1}{2}$, and $\zeta = \frac{1}{4}$ in Eq. (2b) (notice that other equivalent parameterizations are also possible [3], e.g., $\xi = \zeta = 0$, $\eta = \pm 1$ [Eq. (2b)]); as for the model symbol (see also another example in Ref. [2]), notice that potential parameters in the notation of Eq. (2a) assume the values $-1, 0, +1$ so that the symbol 0 or the capital letters are assigned accordingly. Equation (6) now specializes to

$$\Phi = \frac{3}{4}\epsilon \left\{ -s_1(\tilde{\Omega}) + \frac{\sqrt{6}}{3}[s_2(\tilde{\Omega}) + s_3(\tilde{\Omega})] + 2s_4(\tilde{\Omega}) \right\}. \tag{10}$$

The second potential model investigated here (PPM, with the same meaning of symbols as above) is defined by $r_1 = r_2 = +1$, $r_3 = -1$ in the notation of Eq. (2a) and thus takes the form

$$\Phi = \epsilon[G_{11} + G_{22} - G_{33}], \tag{11}$$

corresponding to $\xi=-\frac{1}{2}$, $\eta=0$, $\zeta=+\frac{1}{2}$ in Eq. (2b). Moreover, this potential model enjoys an additional D_{4h} invariance, which means that two simultaneous rotations by $\pm\frac{\pi}{2}$ around the two unit vectors $\mathbf{u}_3$ and $\mathbf{v}_3$, respectively (i.e., taking place in the individual molecular frames), conserve the potential.

The pair ground state configuration for potential models defined by Eq. (9) is essentially unique and can be written down by inspection, also allowing for geometric orthogonality constraints; it reads as

$$\mathbf{v}_1 = \pm\,\mathbf{u}_2, \quad \mathbf{v}_2 = \pm\,\mathbf{u}_1, \quad \mathbf{v}_3 = \pm\,\mathbf{u}_3, \tag{12}$$

where the double signs allow for the D_{2h} symmetry; other critical points can be worked out and invariably lead to a higher energy. Notice also that the bipartite character of the lattice, together with the nearest-neighbor character of the interaction, propagates the pair ground state over the whole lattice without frustration. This configuration entails $\langle s_2\rangle=\langle s_3\rangle=\langle s_4\rangle=0$, whereas both $\langle P_2\rangle$ and its fourth-rank counterpart $\langle P_4\rangle$ equal +1; configurations at sufficiently low temperature are expected to be qualitatively similar to it. MF treatments and MC calculations will be employed to investigate the resulting properties.

It is also appropriate to recall that the chosen parameter values exclude a biaxial ground state on *energy grounds*; on the other hand, the choice

$$\xi = -1, \quad |\eta| \le 1, \quad \zeta = 0 \tag{13}$$

had been investigated as well [2,70] and is known to produce a continuously degenerate pair ground state, excluding biaxiality on *entropy grounds*. Actually, the extreme case $\eta=1$ in Eq. (13) defines model MMP in Ref. [2], i.e., the opposite of the present PPM, and which shows evidence of a second-order uniaxial-to-isotropic transition.

III. MOLECULAR-FIELD ASPECTS

A simple and here rather crude MF procedure (to be called MF1), along the lines of Ref. [2], can be attempted and leads to the following expression for the free energy:

$$A^*_{MF1} = \sigma\sum_{j=1}^{4}\sum_{k=1}^{4} d_{jk}\langle s_j\rangle\langle s_k\rangle - T^*\ln(Z_R) + T^*\ln(8\pi^2), \tag{14}$$

where $\sigma=\rho/2=3$ and $\rho=6$ is the coordination number of the cubic lattice, and

$$Z_R = \int_{Eul} E_R d\omega, \tag{15}$$

$$E_R = \exp(\rho\beta W_R), \tag{16}$$

$$W_R = \sum_{j=1}^{4}\sum_{k=1}^{4} d_{jk}\langle s_j\rangle s_k(\omega), \quad \beta = 1/T^*. \tag{17}$$

Here and in the following, asterisks mean scaling by ϵ for energy quantities or scaling by k_B for specific heats; $\int_{Eul} d\omega$ denotes integration over Euler angles. The symmetric matrix $\mathbf{d}$ with entries d_{jk} is defined by

$$[\mathbf{d}] = \begin{bmatrix} -\xi & 0 & +\frac{\sqrt{6}}{2}\eta & 0 \\ 0 & -2\xi & 0 & +\sqrt{6}\eta \\ +\frac{\sqrt{6}}{2}\eta & 0 & -6\zeta & 0 \\ 0 & +\sqrt{6}\eta & 0 & -12\zeta \end{bmatrix}. \tag{18}$$

Moreover the four consistency conditions

$$\langle s_k\rangle - \frac{1}{Z_R}\int_{Eul} s_k(\omega)\exp(\rho\beta W_R)d\omega = 0, \quad k = 1,2,3,4, \tag{19}$$

entail the extremum equations $\partial A^*_{MF1}/\partial\langle s_j\rangle=0$, $j=1,2,3,4$. The four consistency equations were solved by a numerical bifurcation technique [71,72]; the obtained equilibrium parameters were used to calculate the potential energy per particle U^*_{MF1}

$$U^*_{MF1} = \frac{\partial(\beta A^*_{MF1})}{\partial\beta} = -\sigma\sum_{j,k=1}^{4} d_{jk}\langle s_k\rangle\langle s_j\rangle \tag{20}$$

and hence the specific heat by numerical differentiation. We found for P0M model a low-temperature uniaxially ordered phase characterized by $\langle s_1\rangle>0$, $\langle s_3\rangle>0$ and a first-order transition to the disordered one, taking place at the temperature $\Theta_{MF1}=1.0899$. On the whole, comparisons with MC suggests that MF1 applied to P0M still gives some physically meaningful answer (see also below). On the other hand, when applied to PPM model, this approach simply led to the classical Maier-Saupe model solution, with no effect of the antinematic terms in the pair potential.

Actually, a more refined MF strategy (MF2) can be worked out, taking into proper account the "staggered" structure of the ground state; this is realized at the cost of defining two sets of sublattice order parameters, $\langle p_j\rangle$ and $\langle q_k\rangle$, where p_j and q_k are two different sets of symbols for the four symmetry-adapted basis functions, one for each interpenetrating sublattice; moreover $p_j(\omega)$ have the same functional dependence on ω as $q_j(\omega)$. The *overall* lattice order parameters, which we still denote $\langle s_k\rangle$ as in the previous approximation, will in turn be computed as arithmetic mean of the corresponding pair of sublattice order parameters. In this treatment, the free energy per site would read as

$$A^*_{MF2} = \sigma\sum_{j=1}^{4}\sum_{k=1}^{4} d_{jk}\langle p_j\rangle\langle q_k\rangle - \frac{1}{2}\left[T^*\ln\left(\frac{Z_P}{8\pi^2}\right) + T^*\ln\left(\frac{Z_Q}{8\pi^2}\right)\right], \tag{21}$$

where

$$W_Q = \sum_{j=1}^{4}\sum_{m=1}^{4} d_{jm}\langle q_j\rangle p_m(\omega_1), \quad E_Q = \exp(\rho\beta W_Q),$$

$$Z_Q = \int_{Eul1} E_Q d\omega_1, \tag{22}$$

$$W_P = \sum_{j=1}^{4}\sum_{m=1}^{4} d_{jm}\langle p_j\rangle q_m(\omega_2), \quad E_P = \exp(\rho\beta W_P),$$

$$Z_P = \int_{Eul2} E_P d\omega_2, \tag{23}$$

and the coupling matrix **d** is the same as above; the corresponding resulting consistency equations become

$$\langle p_j\rangle = \frac{\int_{Eul1} p_j(\omega_1) E_Q d\omega_1}{Z_Q}, \quad j = 1,2,3,4, \tag{24}$$

$$\langle q_k\rangle = \frac{\int_{Eul2} q_k(\omega_2) E_P d\omega_2}{Z_P}, \quad k = 1,2,3,4. \tag{25}$$

For any observable f (function depending on Euler angles such as higher-order Legendre-polynomials P_4, etc.), we define

$$\langle f\rangle_Q = \frac{\int_{Eul1} f(\omega_1) E_Q d\omega_1}{Z_Q}, \tag{26}$$

$$\langle f\rangle_P = \frac{\int_{Eul2} f(\omega_2) E_P d\omega_2}{Z_P}, \tag{27}$$

and the resulting overall lattice average is given by

$$\langle f\rangle = \frac{\langle f\rangle_Q + \langle f\rangle_P}{2}. \tag{28}$$

Actually, the MF2 treatment was made computationally more tractable by assuming some physically motivated relations between the two sets of sublattice order parameters, i.e., assuming that the biaxial ones have equal magnitudes and opposite signs in the two sublattices, whereas their uniaxial counterparts have the same value in both sublattices; this ansatz was based on the above pair ground state geometry and consistent with the obtained MC simulation results. Thus, in formulas

$$\langle q_1\rangle = \langle p_1\rangle, \quad \langle q_3\rangle = \langle p_3\rangle, \quad \langle q_2\rangle = -\langle p_2\rangle, \quad \langle q_4\rangle = -\langle p_4\rangle, \tag{29}$$

and in terms of overall lattice order parameters $\langle s_k\rangle$,

$$\langle s_1\rangle = \langle q_1\rangle, \quad \langle s_3\rangle = \langle q_3\rangle, \quad \langle s_2\rangle = \langle s_4\rangle = 0. \tag{30}$$

As could be expected, the MF2 approach was found to lower free energy in comparison with MF1. By the above ansatz, the actually studied system of equations becomes

$$\langle q_k\rangle = \frac{\int_{Eul} q_k(\omega)\exp(\rho\beta W) d\omega}{Z}, \quad k = 1,2,3,4, \tag{31}$$

$$Z = \int_{Eul} \exp(\rho\beta W) d\omega, \tag{32}$$

$$W = -\xi(\langle q_1\rangle q_1 - 2\langle q_2\rangle q_2) - 6\zeta(\langle q_3\rangle q_3 - 2\langle q_4\rangle q_4) + \frac{\sqrt{6}}{2}\eta(\langle q_1\rangle q_3 + \langle q_3\rangle q_1 - 2\langle q_2\rangle q_4 - 2\langle q_4\rangle q_2). \tag{33}$$

The consistency equations were again solved by a numerical bifurcation technique [71,72]; the obtained equilibrium parameters have been used to calculate the potential energy per particle U^*_{MF2}

$$U^*_{MF2} = \frac{\partial(\beta A^*_{MF2})}{\partial\beta} = -\sigma\sum_{j,k=1}^{4} d_{jk}\langle q_k\rangle\langle p_j\rangle \tag{34}$$

and hence the specific heat by numerical differentiation. We again found for P0M model a low-temperature uniaxially ordered phase ($\langle s_1\rangle > 0, \langle s_3\rangle > 0$) and a first-order transition to the disordered one, taking place at the temperature $\Theta_{MF2} = 1.1933$.

When applied to PPM model, MF2 predicted a second-order transition from the isotropic phase to the uniaxial phase taking place at $\Theta_{MF2} = 1.8$. The orientationally ordered equilibrium phase was characterized by a single nonzero (positive) overall uniaxial order parameter, that is, $\langle s_1\rangle > 0$, by vanishing sublattice parameters $\langle p_2\rangle = \langle q_2\rangle = 0$, $\langle p_3\rangle = \langle q_3\rangle = 0$, and by an overall vanishing biaxial order parameter $\langle s_4\rangle$, whereas $\langle p_4\rangle$ and $\langle q_4\rangle$ were different from zero in the ordered phase.

Actually, for the PPM model we tried another ansatz, also consistent with simulation results, i.e., $\langle q_3\rangle = -\langle p_3\rangle$, or more explicitly,

$$\langle q_1\rangle = \langle p_1\rangle, \quad \langle q_3\rangle = -\langle p_3\rangle, \quad \langle q_2\rangle = -\langle p_2\rangle, \quad \langle q_4\rangle = -\langle p_4\rangle. \tag{35}$$

This other approach reproduced the previous overall results and, in addition, yielded a further negative-ordered ($\langle s_1\rangle < 0$) uniaxial solution, now possessing a greater value of free energy than the positive-ordered one. More precisely, this additional solution was characterized by vanishing sublattice biaxial parameters $\langle p_2\rangle = \langle q_2\rangle = 0$, $\langle p_4\rangle = \langle q_4\rangle = 0$, whereas $\langle p_3\rangle = -\langle q_3\rangle \neq 0$ in the ordered phase.

Additional MF2 calculations were carried out for related models generalizing PPM and defined by

$$r_1 = r_2 = +1, \quad r_3 = \tau, \quad \tau \leq -\frac{1}{2}, \tag{36}$$

i.e., $\xi = \frac{1}{2} + \tau$, $\eta = 0$, $\zeta = \frac{1}{2}$ in Eq. (2b). These calculations showed the existence of a tricritical point at $\tau_{tri} = -\frac{19}{17} \approx -1.1176$: the transition between isotropic and uniaxial phases is first order for $\tau \leq \tau_{tri}$ (for a weakly and weakly perturbed Lebwohl-Lasher model) and changes to second order above this threshold, thus remaining second order in a finite neighborhood of the PPM model ($\tau = -1$). Moreover, in the second-order range, the transition temperature is given by

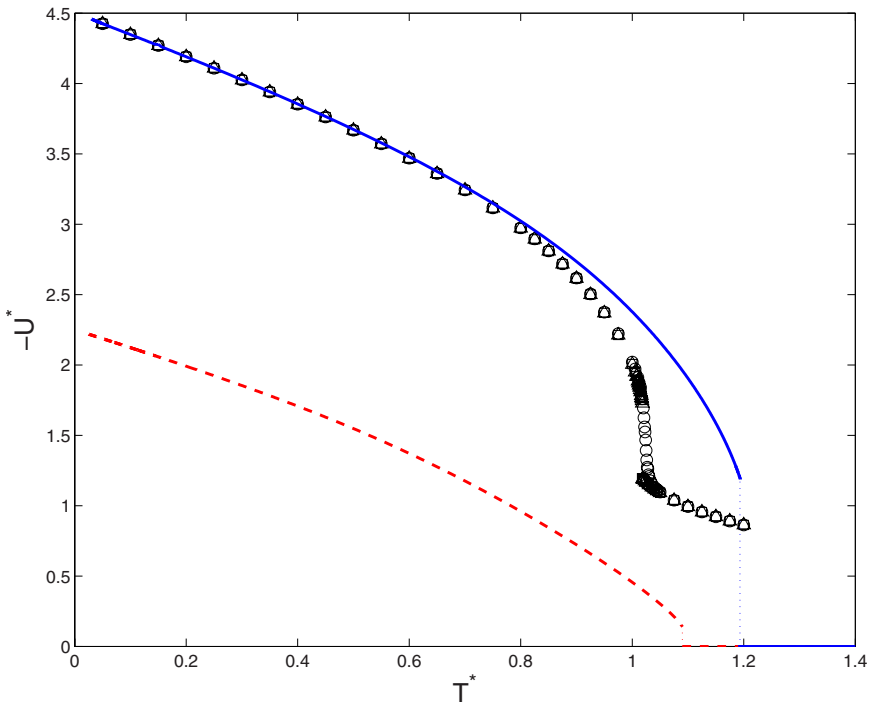

FIG. 1. (Color online) MF1 predictions (red dashed curve), MF2 predictions (blue continuous curve), and simulation results (discrete symbols) for the potential energy, obtained with different sample sizes. As for the meaning of discrete symbols: circles: $l=10$, squares: $l=20$, triangles: $l=30$. Unless explicitly stated or shown, here and in following Figures, error bars fall within symbol sizes.

$$\Theta_{MF2}(\tau) = \frac{9}{5}, \tag{37}$$

i.e., independent of τ. Tricriticality had also been found for other parameter values in Eqs. (1); actually, the change from first–to second order appeared in previously studied models, exhibiting a direct isotropic-to-biaxial phase transition (see Refs. [34,39]).

IV. SIMULATION ASPECTS

The simulation methodology closely follows the one used in our previous papers on the subject [2,38]. Calculations were carried out on a periodically repeated cubic sample, consisting of $N=l^3$ particles with $l=10,20,30$, and were run in cascade, in order of increasing temperature; each cycle (or sweep) consisted of $2N$ MC steps, including a sublattice sweep [73]; the finest temperature steps used were $\Delta T^*=0.001$ and even $\Delta T^*=0.0005$, especially for P0M in the transition regions (see below). Equilibration runs took between 25 000 and 200 000 cycles, and production runs took between 250 000 and 1 250 000; macrostep averages for evaluating statistical errors were taken over 1000 cycles. Calculated thermodynamic quantities include mean potential energy per site U^* and configurational specific heat per particle C^*. Simulation estimates of the overall order parameters $\langle R_{pq}^2 \rangle$ [59,74–76] were calculated by analyzing a configuration every cycle using methodologies discussed in detail by other authors [57,75,77]. We also evaluated the so-called short-range order parameters [74,75]

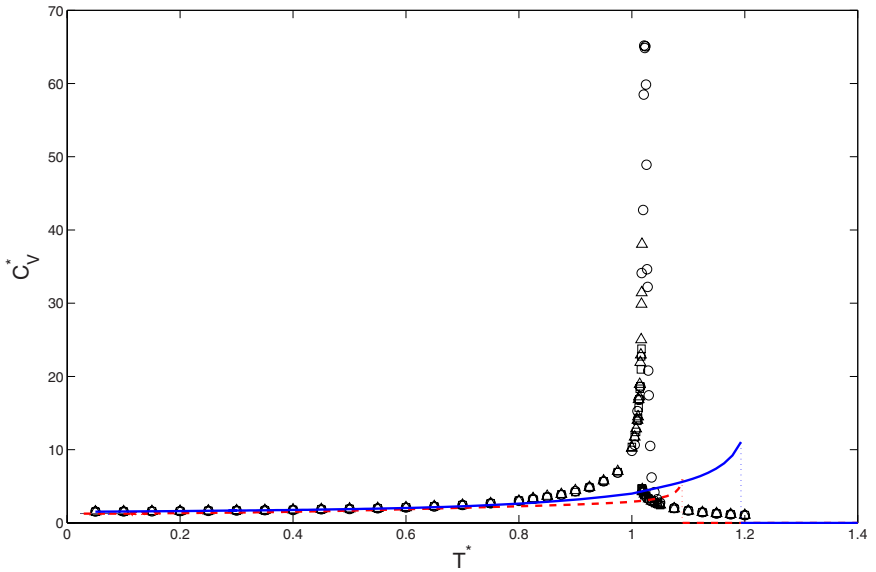

FIG. 2. (Color online) MF predictions and simulation results (discrete symbols) for the configurational specific heat obtained with different sample sizes. Same meaning of symbols as in Fig. 1. Here as well as in Fig. 9, the associated statistical errors, not shown, range up to 2%.

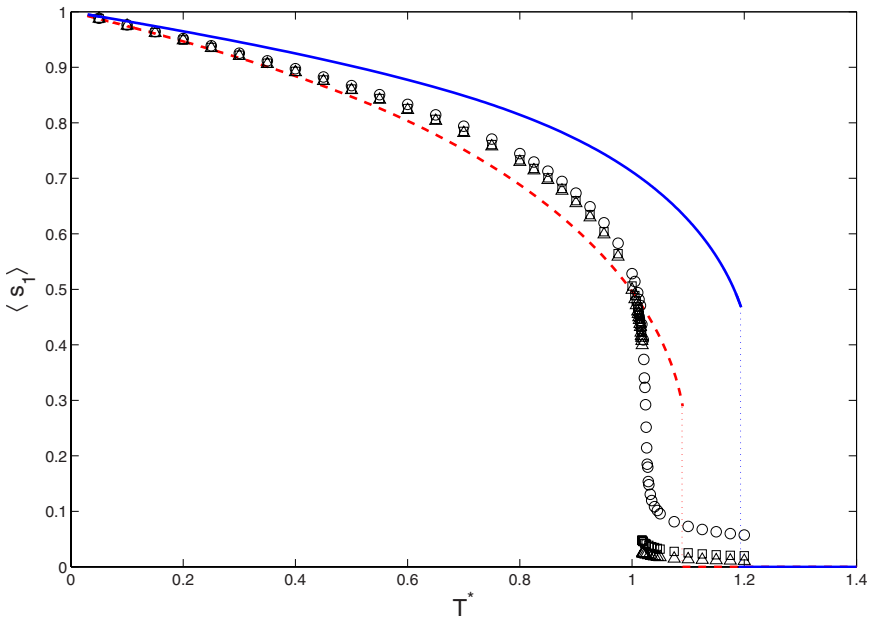

FIG. 3. (Color online) MF predictions and simulation results (discrete symbols) for the overall order parameter $\langle s_1 \rangle$ obtained with different sample sizes. Same meaning of symbols as in Fig. 1.

$$\sigma_{L,j} = \langle P_L(\mathbf{u}_j \cdot \mathbf{v}_j) \rangle, \quad L = 2,4, \quad j = 1,2,3, \tag{38}$$

measuring correlations between corresponding pairs of unit vectors associated with nearest-neighbor molecules; it follows from Eqs. (1) that the potential energy U^* is a linear combination of the quantities $\sigma_{2,j}$. Moreover, for PPM, the D_{4h} symmetry of the pair potential entails that $\sigma_{L,1} = \sigma_{L,2}$. In simulations of this model, at the end of each macrostep, we carried out a rotation of each particle by $\frac{\pi}{2}$ around its $\mathbf{u}_3$ axis [2]; simulation results obtained in this way for $\sigma_{L,j}$ were found to satisfy the above symmetry condition within associated statistical errors.

V. RESULTS AND COMPARISONS

MF predictions and MC results for P0M model and for a few observables are plotted and compared in the following Figs. 1–7; the corresponding comparisons for the PPM counterparts take place in Figs. 8–12.

A. P0M

As for P0M model, simulation results for the potential energy (Fig. 1) were mostly independent of sample size, except for a comparatively narrow temperature range around $T^* \approx 1$, where they showed a pronounced sample-size dependency; actually, already for $l=20$, Fig. 1 showed evidence of a discontinuous jump; moreover, comparison between MF1, MF2, and MC at very low temperatures shows that MF1 only accounts for one half of the ground-state potential energy, whereas MF2 yields the full value. In other words, in this temperature range, one essentially finds the staggered ground state, weakly perturbed by thermal fluctuation, and the named discrepancy reflects the fact that MF1 cannot capture

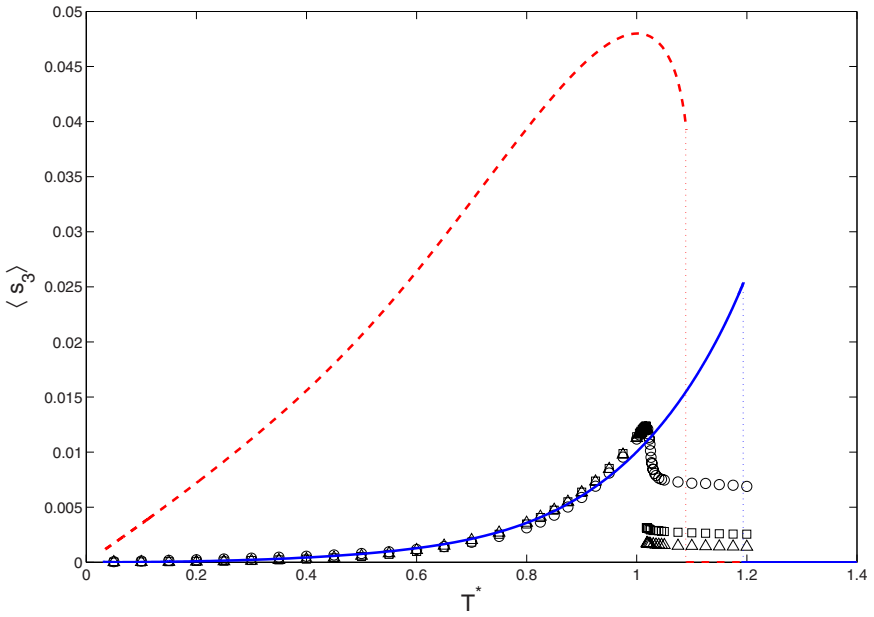

FIG. 4. (Color online) MF predictions and simulation results (discrete symbols) for the overall order parameter $\langle s_3 \rangle$ obtained with different sample sizes; same meaning of symbols as in Fig. 1.

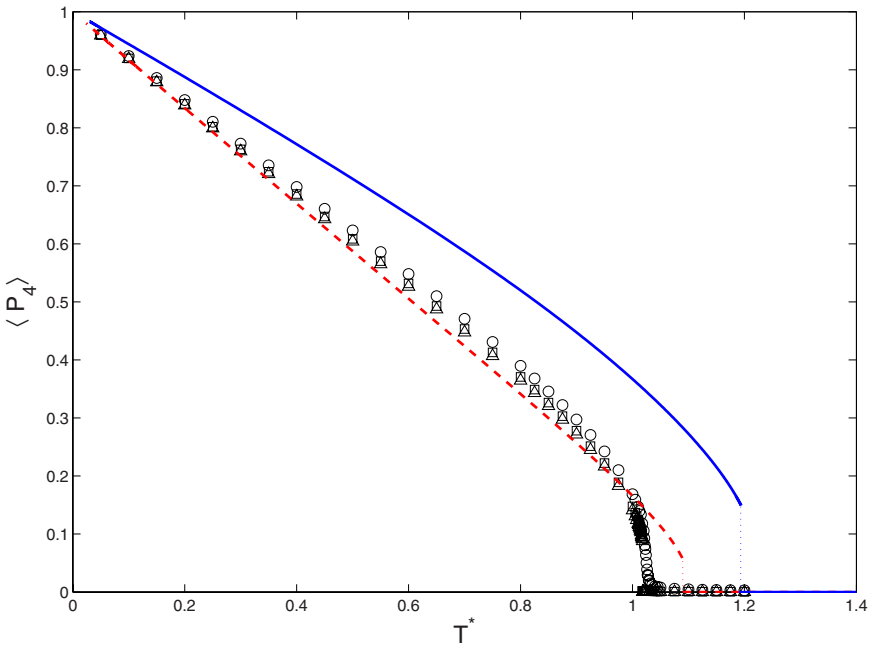

FIG. 5. (Color online) MF predictions and simulation results (discrete symbols) for the overall order parameter $\langle P_4 \rangle$ obtained with different sample sizes; same meaning of symbols as in Fig. 1.

the ground-state structure. The configurational specific heat (Fig. 2) was found to be independent of sample size for $T^* \leq 0.975$ and then for $T^* \geq 1.05$ and exhibited a recognizable sample-size dependency in between, where the peak appeared to narrow with increasing sample size. As for $\langle s_1 \rangle$, Fig. 3 shows evidence of a jump, taking place at the same temperature as for U^* and developing as system size increases; on the other hand, in the low-temperature régime, sample-size effects appear to saturate for $l \geq 20$, whereas the high-temperature region exhibits a pronounced decrease in $\langle s_1 \rangle$ with increasing sample size; Fig. 4 showed a similar scaling behavior as for $\langle s_3 \rangle$; moreover, both MF2 and MC results exhibited a monotonic increase up to the transition temperature, in contrast with the maximum predicted by MF1.

Simulation results for the overall biaxial order parameters $\langle s_2 \rangle$ and $\langle s_4 \rangle$ (not shown) were found to be rather small ($\langle s_2 \rangle \leq 0.03, \langle s_4 \rangle \leq 0.006$) and kept decreasing with increasing sample size, in agreement with the overall uniaxial behavior. Simulation results for $\langle P_4 \rangle$ (Fig. 5) showed a pattern similar to $\langle s_1 \rangle$. On the whole, MF1 provided acceptable temperature profiles for the order parameters $\langle s_1 \rangle$ as well as $\langle P_4 \rangle$ (see Figs. 3 and 5); on the other hand, it overestimated the order parameter $\langle s_3 \rangle$ by a few times and missed its overall temperature behavior (Fig. 4); in other words, it just mimicked the gross effect of nematic coupling.

Simulation results for the short-range order parameters $\sigma_{2,j}$ and $\sigma_{4,j}$ obtained with the largest sample size $l=30$ are plotted in Figs. 6 and 7; they show a monotonic evolution with temperature and evidence of a jump at $T^* \approx 1$, in agree-

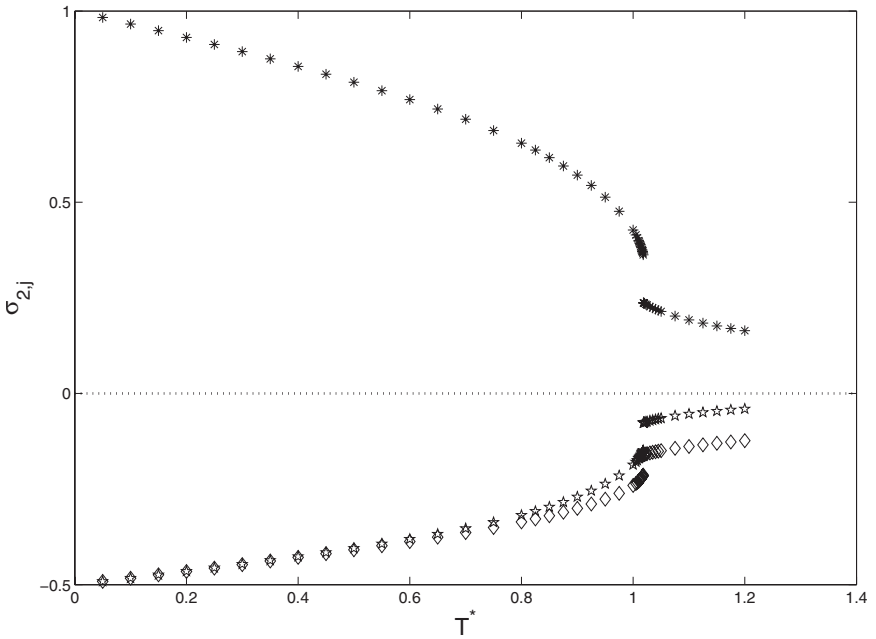

FIG. 6. Simulation results for the short-range order parameters $\sigma_{2,j}$ obtained with sample size $l=30$. As for the meaning of symbols: diamonds: $\sigma_{2,1}$; stars: $\sigma_{2,2}$; asterisks: $\sigma_{2,3}$.

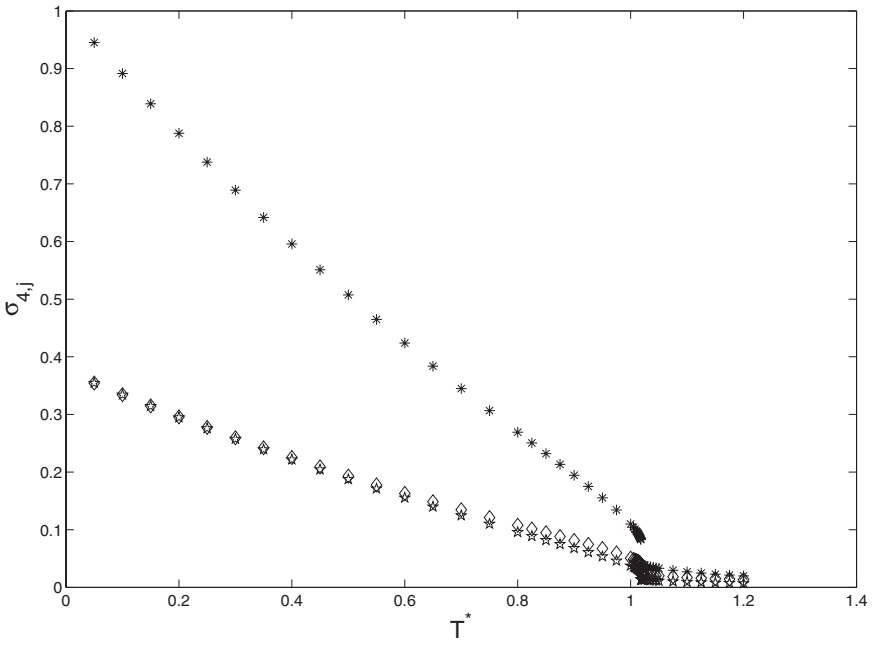

FIG. 7. Simulation results for the short-range order parameters $\sigma_{4,j}$ obtained with sample size $l=30$; same meaning of symbols as in Fig. 6.

ment with the above observables; their sample-size dependency, not shown, parallels the one observed for U^*. Notice also that each $\sigma_{L,2}$, i.e., a quantity involving axes not directly coupled by the interaction, remains close to the corresponding $\sigma_{L,1}$, especially in the ordered region, and has consistently the smallest magnitude among the three $\sigma_{L,j}$ as could be expected.

Thus we propose a first-order transition and the value $\Theta_{MC}=1.018\pm0.001$ for the transition temperature; here the error bar is conservatively taken to be twice the temperature step used in the transition region. Upon analyzing the simulation results for the largest sample as discussed in Refs. [78,79], we obtained the estimates for transitional properties collected in Table I; actually, the same analysis was also applied to simulation results obtained for $l=20$, and yielded comparable results. Table I shows a fair qualitative agreement between MF and MC; of course, in quantitative terms MF overestimates the transition temperature and, even worse, its first-order character, as well known for LL; let us mention, for comparison, that the ratio Θ_{MC}/Θ_{MF} is ≈0.934 as predicted by the simple MF1 treatment and ≈0.853 as for the refined one MF2 and that the corresponding value for LL is ≈0.856 [46]. On the whole, comparisons between MF1, MF2, and MC, show that MF2 produces a significantly better qualitative agreement with MC (see especially Fig. 1); this can be expected and understood since MF1 is actually appropriate for uniform biaxial order. On the other hand, Table I also shows that MF1 and MF2 estimates for such transitional properties as ΔU^*, $\langle s_1\rangle$, $\langle P_4\rangle$, bracket the corresponding MC results from below (MF1) and from above (MF2), whereas both MF1 and MF2 overestimate Θ as well as $\langle s_3\rangle$.

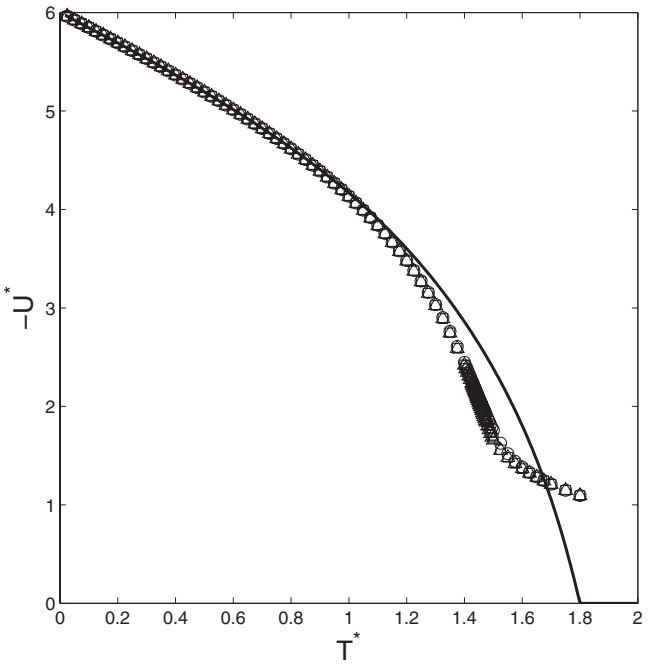

FIG. 8. MF2 predictions (continuous curve) and simulation results (discrete symbols) for the potential energy obtained with different sample sizes. As for the meaning of discrete symbols: circles: $l=10$, squares: $l=20$, triangles: $l=30$.

B. PPM

Simulations were first carried out using a minimum temperature step of 0.0025 and suggested a continuous transition taking place somewhere between $T^*=1.45$ and $T^*=1.46$; additional simulations were then carried out in the named temperature range, using an even finer temperature step, down to 0.0005 and essentially confirmed the above picture; the latter results were not plotted for reasons of readability; notice also, for comparison, that in the previous P0M case, usage of a very fine temperature step had enabled us to pinpoint the transition. MF predictions and MC results for PPM and for a few observables are plotted and compared in the following Figs. 8–12. Simulation results for the potential energy (Fig. 8) were found to change with temperature in a gradual and

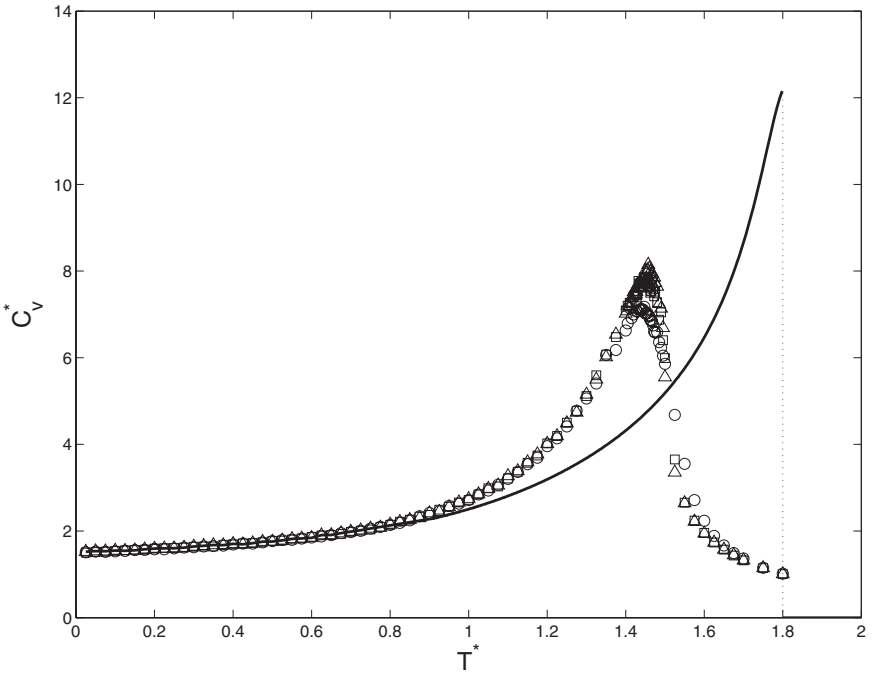

FIG. 9. MF2 predictions (continuous curve) and simulation results (discrete symbols) for the configurational specific heat obtained with different sample sizes. Same meaning of symbols as in Fig. 8.

monotonic way; a rather weak sample-size dependency was found to take place around $T^* \approx 1.45$ and to saturate for $l \geq 20$. Results for the configurational specific heat (Fig. 9) were found to be independent of sample size for $T^* \leq 1.4$ and then again for $T^* \geq 1.6$ and exhibited a more recognizable but not very pronounced sample-size dependency in between, where they peaked at $T^* \approx 1.45$.

As for $\langle s_1 \rangle$, Fig. 10 shows a gradual and monotonic decay with increasing temperature; at $T^* \leq 1.4$ sample-size dependency appears to saturate for $l \geq 20$, whereas the higher temperature region exhibits a pronounced decrease in $\langle s_1 \rangle$ with increasing sample size; on the whole, upon increasing the sample size, the MC results recognizably point to a continuous vanishing at $T^* \approx 1.45$, where the specific heat attains its maximum. Simulation results for the three order parameters $\langle s_2 \rangle$, $\langle s_3 \rangle$, and $\langle s_4 \rangle$ (not shown) were found to be rather small ($\langle s_2 \rangle \leq 0.03$, and the other two did not exceed 0.005) and to exhibit a pronounced decrease with increasing sample size, in agreement with the overall MF prediction. Simulation results for $\langle P_4 \rangle$ (Fig. 11) showed a pattern similar to $\langle s_1 \rangle$. Simulation results for the short-range order parameters $\sigma_{2,j}$ and $\sigma_{4,j}$ obtained with the largest sample size $l=30$ are plotted in Fig. 12; they show a gradual and monotonic decay with temperature.

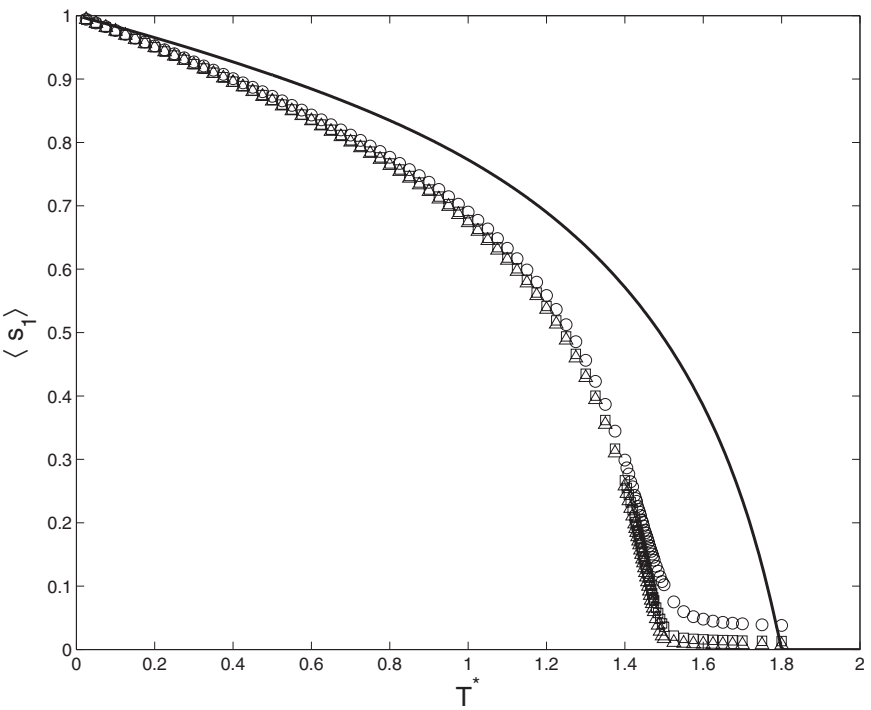

FIG. 10. MF2 predictions (continuous curve) and simulation results (discrete symbols) for the overall order parameter $\langle s_1 \rangle$ obtained with different sample sizes. Same meaning of symbols as in Fig. 8.

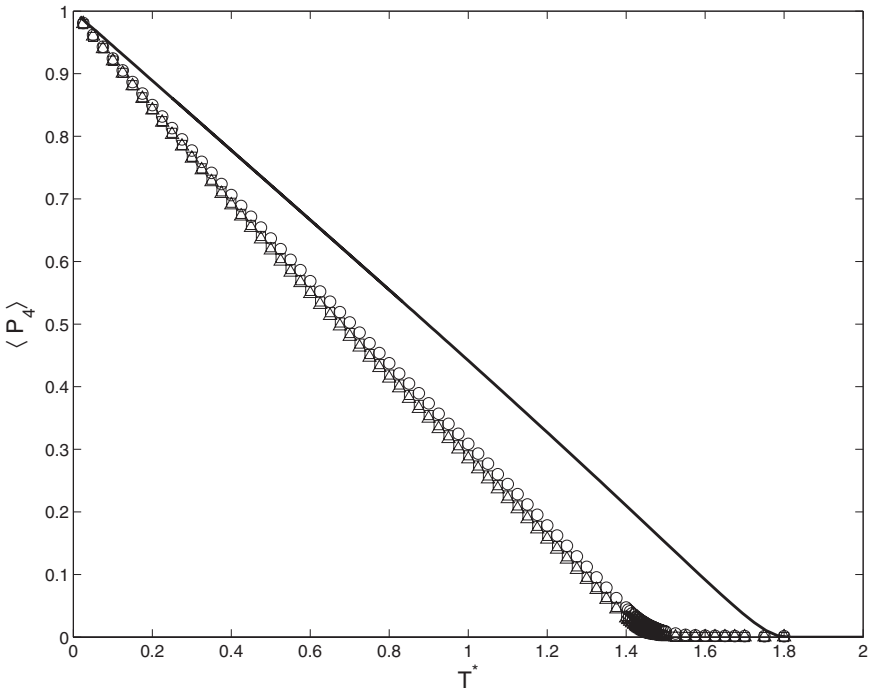

FIG. 11. MF2 predictions (continuous curve) and simulation results (discrete symbols) for the overall order parameter $\langle P_4 \rangle$ obtained with different sample sizes; same meaning of symbols as in Fig. 8.

Thus we propose a second-order transition and conservatively estimate the transition temperature to be $\Theta_{MC} = 1.455 \pm 0.005$, hence the ratio $\Theta_{MC}/\Theta_{MF} \approx 0.81$; let us also recall that model MMP studied in Ref. [2] (i.e., the opposite of the present PPM) produces no biaxial order (via an entropic mechanism) and a second-order isotropic-to-nematic transition as well, with a ratio $\Theta_{MC}/\Theta_{MF} \approx 0.6$. In experimental terms, the uniaxial nematic-to-isotropic transition is usually weakly first order, but some rare example showing evidence of tricritical behavior in a nearly second-order case has been reported in Ref. [80] where a cyclic liquid crystalline trimer has been employed.

VI. SUMMARY AND OUTLOOK

As already pointed out, nematogenic molecules do not usually possess uniaxial ($D_{\infty h}$) symmetry, but their resulting mesophases *often* do. On the other hand, the pair potential model in Eq. (2a) or Eq. (2b) has proven to be simple but rather versatile and can produce a biaxial pair ground state under certain appropriate ranges of parameters; we have therefore chosen to investigate some other ranges of parameters, producing a uniaxial (pair) ground state, thus precluding a biaxial phase on energy grounds. The chosen parameter values entail a nematic coupling between the long molecular

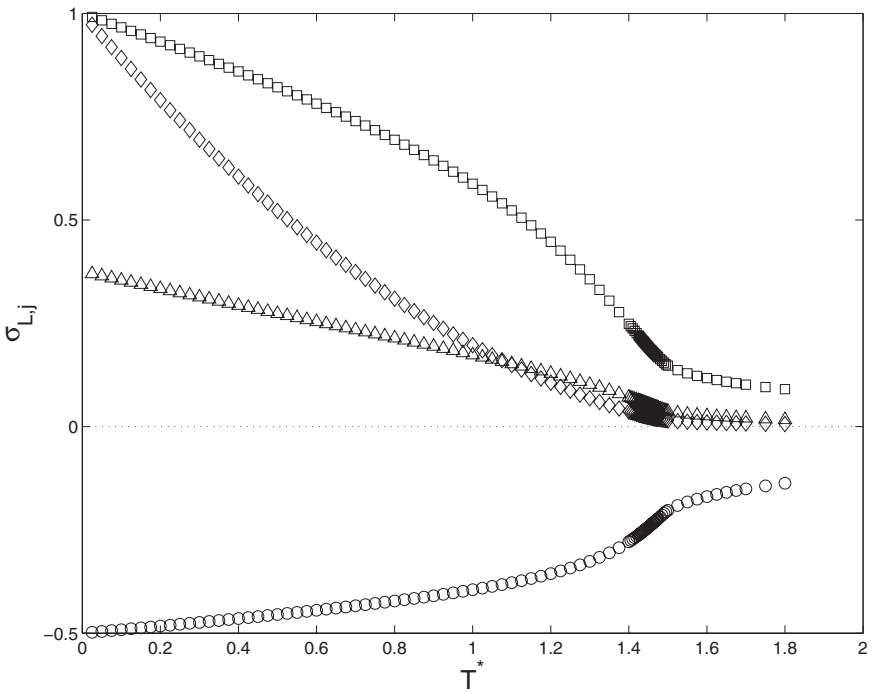

FIG. 12. Simulation results for the short-range order parameters $\sigma_{2,j}$ and $\sigma_{4,j}$, obtained with sample size $l=30$. As for the meaning of symbols: circles: common value of $\sigma_{2,1}$ and $\sigma_{2,2}$; squares: $\sigma_{2,3}$; triangles: common value of $\sigma_{4,1}$ and $\sigma_{4,2}$; diamonds: $\sigma_{4,3}$.

TABLE I. Transitional properties for the investigated model P0M: MC results are based on the largest investigated sample size $l=30$.

Method	Θ	$\langle s_1 \rangle$	$\langle s_3 \rangle$	ΔU^*	$\langle P_4 \rangle$
MF1	1.0899	0.2900	0.0393	0.1404	0.0561
MC	1.018 ± 0.001	0.40 ± 0.01	0.01210 ± 0.00004	0.54 ± 0.02	0.088 ± 0.005
MF2	1.1933	0.4686	0.0253	1.0773	0.1495

axes, and an antinematic one between other corresponding axes. The two selected potential models were examined by MF and MC; the simple MF1 approach [2] (actually appropriate for homogeneous *biaxial* order) was found to give a rather crude answer for P0M, whereas its usage for PPM simply missed the relevant points. A more refined treatment (MF2) was developed, now taking into proper account the structure of the pair ground state and yielding results in reasonable and improved qualitative agreement with simulation for both potential models. Notice that both PPM and its opposite MMP [2] produced a second-order isotropic-to-uniaxial transition; for MMP this behavior seems to be linked with an additional ground-state degeneracy; on the other hand, the above MF2 results suggest this to happen for the related potential models defined by Eq. (36), over a finite parameter range $-\frac{19}{17} < \tau \leq -\frac{1}{2}$. Notice that Eqs. (1) can also produce second-order transitions between an ordered biaxial phase and the isotropic one for other suitable parameter values [34,39]: all these cases appear to require $r_1=r_2$ (or $\eta=0$) and comparable values of $|r_1|$ and $|r_3|$; these conditions were usually not met in the earlier studies, addressing Straley or dispersionlike models (see Sec. II); in turn, these conditions may entail rather severe constraints in terms of molecular architecture and molecular interactions. At any rate, this unusual behavior (see also above) appears to deserve a fresh investigation (see also the remarks in Ref. [4] about other "missing" phases).

Some other piece of information can be obtained or, at least, guessed for the investigated family of potential models. On the one hand, one can consider a lattice with a different coordination, more specifically a diamond lattice (where the nearest neighbors of a lattice site are also nearest neighbors to each other) or, in general, a model where particle centers of mass move in $\mathbb{R}^3$, and more distant neighbors are involved in the interaction, possessing the same angular form as above, but modulated by a positive decreasing function of the distance between them. In this case, all calamitic pair interactions can be simultaneously minimized but not all antinematic ones; this situation should reduce the absolute values of the corresponding $\sigma_{2,j}$ terms; in pictorial terms, this energy-based mechanism (see Refs. [2,70] for its entropic counterpart) would tend to enforce "effective uniaxial" symmetry of the molecules.

On the other hand, one can conceive other models (PP0, PPP) where the calamitic term has been eliminated so that the pair ground state cannot even be uniaxial, in pronounced contrast with the situations observed in previous cases. In these instances, already at the level of preliminary calculations, *qualitatively* different scenarios start emerging: for example, the pair ground state of PPP is doubly degenerate, its overall ground state is also significantly degenerate but not frustrated and exhibits no second-rank orientational order but fourth-rank cubatic one (actually, the condition $r_1=r_2=r_3$ entails O_h symmetry of the interaction). Moreover, in the very low temperature limit, one can think of neglecting fluctuations, hence consider discretized particle orientations and thus make some contact with the antiferromagnetic three-state Potts model [81]. This study is in progress and will be reported in due course.

ACKNOWLEDGMENTS

The present extensive calculations were carried out, on among other machines, workstations, belonging to the Sezione di Pavia of Istituto Nazionale di Fisica Nucleare (INFN); allocations of computer time by the Computer Centre of Pavia University and CILEA (Consorzio Interuniversitario Lombardo per l' Elaborazione Automatica, Segrate-Milan), as well as by CINECA (Centro Interuniversitario Nord-Est di Calcolo Automatico, Casalecchio di Reno-Bologna), are gratefully acknowledged. The authors also wish to thank Professor L. Longa (Krakow, Poland), Professor G. R. Luckhurst and Professor T. J. Sluckin (Southampton, England, UK), and Professor E. G. Virga (Pavia, Italy) for helpful discussion and suggestions.

[1] M. J. Freiser, Phys. Rev. Lett. **24**, 1041 (1970).
[2] G. De Matteis and S. Romano, Phys. Rev. E **78**, 021702 (2008).
[3] S. Romano, Physica A **337**, 505 (2004).
[4] R. Berardi, L. Muccioli, S. Orlandi, M. Ricci, and C. Zannoni, J. Phys.: Condens. Matter **20**, 463101 (2008).
[5] M. A. Bates, Phys. Rev. E **74**, 061702 (2006).
[6] L. Longa, G. Pająk, and T. Wydro, Phys. Rev. E **79**, 040701(R) (2009).
[7] J. Peláez and M. R. Wilson, Phys. Rev. Lett. **97**, 267801 (2006).
[8] L. J. Yu and A. Saupe, Phys. Rev. Lett. **45**, 1000 (1980).
[9] G. R. Luckhurst, Thin Solid Films **393**, 40 (2001).
[10] K. Praefcke, Mol. Cryst. Liq. Cryst. Sci. Technol., Sect. A **364**, 15 (2001).
[11] K. Praefcke, Braz. J. Phys. **32**, 564 (2002).

[12] G. R. Luckhurst, Angew. Chem., Int. Ed. **44**, 2834 (2005).
[13] L. A. Madsen, T. J. Dingemans, M. Nakata, and E. T. Samulski, Phys. Rev. Lett. **92**, 145505 (2004).
[14] B. R. Acharya, A. Primak, and S. Kumar, Phys. Rev. Lett. **92**, 145506 (2004).
[15] J. You, J. Y. Jung, K. Rhie, V. M. Pergamenshchik, and S. T. Shin, J. Korean Phys. Soc. **52**, 342 (2008).
[16] V. Görtz, C. Southern, N. W. Roberts, H. F. Gleeson, and J. W. Goodby, Soft Matter **5**, 463 (2009).
[17] Y. Galerne, Phys. Rev. Lett. **96**, 219803 (2006).
[18] L. A. Madsen, T. J. Dingemans, M. Nakata, and E. T. Samulski, Phys. Rev. Lett. **96**, 219804 (2006).
[19] K. Merkel, A. Kocot, J. K. Vij, R. Korlacki, G. H. Mehl, and T. Meyer, Phys. Rev. Lett. **93**, 237801 (2004).
[20] J. L. Figueirinhas, C. Cruz, D. Filip, G. Feio, A. C. Ribeiro, Y. Frère, T. Meyer, and G. H. Mehl, Phys. Rev. Lett. **94**, 107802 (2005).
[21] C. Cruz, J. L. Figueirinhas, D. Filip, G. Feio, A. C. Ribeiro, Y. Frère, T. Meyer, and G. H. Mehl, Phys. Rev. E **78**, 051702 (2008).
[22] G. Cordoyiannis, D. Apreutesei, G. H. Mehl, C. Glorieux, and J. Thoen, Phys. Rev. E **78**, 011708 (2008).
[23] K. Neupane, S. W. Kang, S. Sharma, D. Carney, T. Meyer, G. H. Mehl, D. W. Allender, S. Kumar, and S. Sprunt, Phys. Rev. Lett. **97**, 207802 (2006).
[24] F. Hessel and H. Finkelmann, Polym. Bull. (Berlin) **15**, 349 (1986).
[25] K. Severing and K. Saalwächter, Phys. Rev. Lett. **92**, 125501 (2004).
[26] K. Severing, E. Stibal-Fischer, A. Hasenhindl, H. Finkelmann, and K. Saalwächter, J. Phys. Chem. B **110**, 15680 (2006).
[27] V. Cîrcu, P. N. Horton, M. B. Hursthouse, and D. W. Bruce, Liq. Cryst. **34**, 1463 (2007).
[28] A. G. Vanakaras and D. J. Photinos, J. Chem. Phys. **128**, 154512 (2008).
[29] G. R. Luckhurst, Nature (London) **430**, 413 (2004).
[30] G. R. Luckhurst, British Liquid Crystal Society Newsletter, August, 10 (2005). See http://www-g.eng.cam.ac.uk/blcs/
[31] J.-H. Lee, T.-K. Lim, W.-T. Kim, and J.-I. Jin, J. Appl. Phys. **101**, 034105 (2007).
[32] R. Berardi, L. Muccioli, and C. Zannoni, J. Chem. Phys. **128**, 024905 (2008).
[33] A. M. Sonnet, E. G. Virga, and G. E. Durand, Phys. Rev. E **67**, 061701 (2003).
[34] G. De Matteis and E. G. Virga, Phys. Rev. E **71**, 061703 (2005).
[35] F. Bisi, E. G. Virga, E. C. Gartland, Jr., G. De Matteis, A. M. Sonnet, and G. E. Durand, Phys. Rev. E **73**, 051709 (2006).
[36] G. De Matteis, F. Bisi, and E. G. Virga, Continuum Mech. Thermodyn. **19**, 1 (2007).
[37] R. Rosso and E. G. Virga, Phys. Rev. E **74**, 021712 (2006).
[38] S. Romano, Phys. Lett. A **333**, 110 (2004).
[39] G. De Matteis, S. Romano, and E. G. Virga, Phys. Rev. E **72**, 041706 (2005).
[40] Z.-D. Zhang, Y.-J. Zhang, and Z.-L. Sun, Chin. Phys. Lett. **23**, 3025 (2006).
[41] D. Allender and L. Longa, Phys. Rev. E **78**, 011704 (2008).
[42] G. De Matteis, A. M. Sonnet, and E. G. Virga, Continuum Mech. Thermodyn. **20**, 347 (2008).
[43] B. Mettout, Phys. Rev. E **72**, 031706 (2005).
[44] B. Mettout, P. Tolédano, H. Takezoe, and J. Watanabe, Phys. Rev. E **66**, 031701 (2002).
[45] B. Mettout, Phys. Rev. E **74**, 041701 (2006).
[46] P. Pasini, C. Chiccoli, and C. Zannoni, in *NATO Science Series C*, edited by P. Pasini and C. Zannoni (Kluwer, Dordrecht, 2000), Vol. 545, Chap. 5.
[47] M. A. Bates and G. R. Luckhurst, Phys. Rev. E **72**, 051702 (2005).
[48] G. Lasher, Phys. Rev. A **5**, 1350 (1972).
[49] P. I. C. Teixeira, M. A. Osipov, and G. R. Luckhurst, Phys. Rev. E **73**, 061708 (2006).
[50] Y. Martinez-Ratón, S. Varga, and E. Velasco, Phys. Rev. E **78**, 031705 (2008).
[51] C. Chiccoli, P. Pasini, F. Semeria, and C. Zannoni, Int. J. Mod. Phys. C **10**, 469 (1999).
[52] D. M. Brink and G. R. Satchler, *Angular Momentum*, 2nd ed. (Oxford University Press, Oxford, England, 1968).
[53] D. A. Varshalovich, A. N. Moskalev, and V. K. Khersonskii, *Quantum Theory of Angular Momentum* (World Scientific, Singapore, 1988).
[54] G. B. Arfken and H. J. Weber, *Mathematical Methods for Physicists*, 4th ed. (Academic Press, San Diego, 1995).
[55] J. P. Straley, Phys. Rev. A **10**, 1881 (1974).
[56] G. R. Luckhurst, C. Zannoni, P. L. Nordio, and U. Segre, Mol. Phys. **30**, 1345 (1975).
[57] F. Biscarini, C. Chiccoli, P. Pasini, F. Semeria, and C. Zannoni, Phys. Rev. Lett. **75**, 1803 (1995).
[58] B. Mulder, Phys. Rev. A **39**, 360 (1989).
[59] R. Rosso, Liq. Cryst. **34**, 737 (2007).
[60] A. D. Buckingham, in *Advances in Chemical Physics*, edited by J. O. Hirschfelder (Interscience, New York, 1967), Vol. 12, Chap. 2, pp. 107–142.
[61] C. G. Gray and K. E. Gubbins, *Theory of Molecular Fluids* (Oxford University Press, Oxford, UK, 1984), Vol. 1.
[62] B. Bergersen, P. Palffy-Muhoray, and D. A. Dunmur, Liq. Cryst. **3**, 347 (1988).
[63] S. Romano, Physica A **339**, 511 (2004).
[64] S. Romano, Physica A **339**, 491 (2004).
[65] R. F. Kayser, Jr. and H. J. Raveché, Phys. Rev. A **17**, 2067 (1978).
[66] L. Longa, P. Grzybowski, S. Romano, and E. Virga, Phys. Rev. E **71**, 051714 (2005); **73**, 019904(E) (2006).
[67] L. Longa and G. Pajak, Liq. Cryst. **32**, 1409 (2005).
[68] F. Bisi, S. Romano, and E. G. Virga, Phys. Rev. E **75**, 041705 (2007).
[69] F. Bisi, G. R. Luckhurst, and E. G. Virga, Phys. Rev. E **78**, 021710 (2008).
[70] G. R. Luckhurst and S. Romano, Mol. Phys. **40**, 129 (1980).
[71] J. F. Willy, *Govaerts, Numerical Methods for Bifurcations of Dynamical Equilibria* (SIAM, Philadelphia, 2000).
[72] The bifurcation analysis has been performed by using an AUTO-2000 package: E. Doedel, R. C. Paffenroth, A. R. Champneys, T. F. Fairgrieve, Y. A. Kuznetsov, B. E. Oldeman, B. Sandstede, and X. Wang, *AUTO2000: Continuation and bifurcation software for ordinary differential equations (with HOMCONT)*, Technical report, Concordia University, 2002. See also webpage http://auto2000.sourceforge.net/
[73] R. Hashim and S. Romano, Int. J. Mod. Phys. B **13**, 3879 (1999).
[74] C. Zannoni, in *The Molecular Physics of Liquid Crystals*, ed-

ited by G. R. Luckhurst and G. W. Gray (Academic Press, London, 1979), Chaps. 3 and 9.
[75] C. Zannoni, in *NATO Science Series C*, edited by P. Pasini and C. Zannoni (Kluwer, Dordrecht, 2000), Vol. 545, Chap. 2.
[76] G. R. Luckhurst, in *Physical Properties of Liquid Crystals: Nematics*, edited by D. A. Dunmur, A. Fukuda, and G. R. Luckhurst (INSPEC, London, 2001), Chap. 2.1.
[77] M. P. Allen, Liq. Cryst. **8**, 499 (1990).
[78] S. Romano, Int. J. Mod. Phys. B **16**, 2901 (2002).
[79] S. Romano, Physica A **324**, 606 (2003).
[80] I. M. Syed, V. Percec, R. G. Petschek, and C. Rosenblatt, Phys. Rev. E **67**, 011704 (2003).
[81] F. Y. Wu, Rev. Mod. Phys. **54**, 235 (1982).